Magn Reson Mater Phy (2008) 21:307–315
DOI 10.1007/s10334-008-0131-5

RESEARCH ARTICLE

Flow-compensated self-gating

Jessica Schulz · Matthias Korn · Michael Deimling · Wolfhard Semmler · Michael Bock

Received: 29 April 2008 / Revised: 15 July 2008 / Accepted: 16 July 2008 / Published online: 31 July 2008

Abstract
Objective Self-gating (SG) is a method to record cardiac movement during MR imaging. It uses information from an additional short, non-spatially encoded data acquisition. This usually lengthens TE and increases the sensitivity to flow artifacts. A new flow compensation scheme optimized for self-gating sequences is introduced that has very little or no time penalty over self-gating sequences without flow compensation.
Materials and methods Three variants of a self-gated 2D spoiled gradient echo or fast low angle shot (FLASH) sequence were implemented: without (noFC), with a conventional, serial (cFC), and with a new, time-efficient flow compensation (sFC). In experiments on volunteers and small animals, the sequence variants were compared with regard to the SG signal and the flow artifacts in the images.
Results Both cFC and sFC reduce flow artifacts in cardiac images. The SG signal of the sFC is more sensitive to physiological motion, so that a cardiac trigger can be extracted more precisely as in cFC. In a typical setting for small animal imaging, sFC technique reduces the echo/repetition time over cFC by about 23%/14%.
Conclusion The time-efficient sFC technique provides flow-compensated images with cardiac triggering in both volunteers and small animals.

Keywords Self-gating · Self-navigation · Flow compensation · Small animal imaging

J. Schulz · M. Deimling
Siemens Medical Solutions, Erlangen, Germany

J. Schulz · M. Korn · W. Semmler · M. Bock (✉)
Deutsches Krebsforschungszentrum (dkfz), Abt. Medizinische Physik in der Radiologie (E020), Im Neuenheimer Feld 280, 69120 Heidelberg, Germany
e-mail: m.bock@dkfz.de

Introduction

In magnetic resonance imaging (MRI), the fact that the timescale for image acquisition is usually longer than the timescale for physiological movements results in images contaminated with motion artifacts. To obtain artifact-free cardiac images it is necessary to either synchronize the image acquisition prospectively with the cardiac movement, or to retrospectively sort the image data with respect to the phases of the cardiac cycle. In either case, heart movement of the patient needs to be recorded during the measurement. For this, typically the ECG-signal is used either for triggering or for gating.

The measurement of the ECG-signal during MRI can be challenging for several reasons. Magnetically induced voltages can distort the ECG signals which originate either from the magnetohydrodynamic effect [1–3] (i.e., moving ions in blood are deflected in the main magnetic field), from the switching of the imaging gradients, or the RF pulsing [4–8]. These effects become more pronounced at higher field strengths and gradient strengths. Secondly, the positioning of the ECG electrodes is a time-consuming process that prolongs preparation of either patient or animal. Also, patient-related arrhythmia or large variations in heart rate during image acquisition may lead to erroneous R-wave detection [9]. In small animals it is especially difficult to acquire a good trigger signal because the voltage differences are small and, additionally, the presence of fur might hamper the placement of the electrodes. Furthermore, ECG triggering units use filters to suppress noise in the ECG signal—if the time constants in these filters are not adapted to the length of the RR interval, the system cannot be used for both human and small animal experiments. In addition, the long wires and the electrodes of the ECG system can be hazardous for the patient during RF transmission [10].

An alternative method to derive a cardiac trigger uses the MR signal itself. Here, for each acquisition an additional MR signal without gradient encoding is acquired for triggering. This self-gating (SG) signal shows temporal variations that are correlated with the cardiac and the respiratory cycle, which is especially pronounced when the slice is intersecting with the heart [11,12]. The variations are caused by inflow of unsaturated spins (time-of-flight effect) and velocity-dependent phase changes (phase contrast).

Self-gating trigger times are often calculated by a signal peak detection algorithm. To improve the accuracy of trigger detection, Nijm et al. [13] used a template matching algorithm that computes the cross-correlation of an SG template function with the measured sample. The trigger positions are then defined as the peaks of the cross-correlation signal. They could show that this algorithm is more precise than a simple sign change detection in the first derivative of the SG time curve, which identifies the peaks in the SG signal.

Self-gating has been favorably combined with radial k-space acquisitions where the central k-space point, which is not spatially encoded, is automatically acquired for each radial projection [14]. For Cartesian k-space sampling two separate acquisitions are required for the SG signal and the image data which leads to a slightly prolonged total acquisition time; however, comparison of radial and Cartesian SG techniques in small animal data using high field systems showed that Cartesian sampling delivers the more robust SG signal [15].

In cardiac imaging, both blood flow and respiratory motion can cause artifacts. Flow artifacts can be partially reduced by introducing flow compensating gradients into the pulse sequence which null higher order gradient moments (typically, the first moment only) at the time of the data acquisition [16–18]. This reduces signal loss and ghosting image artifacts that occur when there is pulsatile flow or periodic motion. Also, intravoxel phase dispersion that occurs when there is a range of flow velocities within a single voxel are eliminated or reduced [19]. Flow compensation requires additional time between radio-frequency (rf) excitation and data acquisition, so that echo times and repetition times are increased. With increasing echo time higher order gradient moments grow, and the pulse sequence becomes more sensitive to secondary motion effects such as acceleration. Due to the prolongation of TE, Cartesian SG sequences show an increased sensitivity to flow artifacts and flow-compensation might be necessary.

In this article, we implemented two strategies for flow compensation in a 2D spoiled gradient echo or fast low angle shot (FLASH) SG sequence: a longer serial flow compensation, and a shorter time-efficient implementation. The two flow compensation strategies were compared in both humans and small animals with a SG sequence without flow compensation.

Materials and methods

2D FLASH SG sequence

A Cartesian 2D FLASH SG pulse sequence was implemented on a clinical 1.5 T MR system (Siemens Symphony, Erlangen, Germany) equipped with a Quantum gradient system ($G_{\max} = 30\,\text{mT/m}$, $s_{\max} = 100\,\text{mT/m/ms}$). A schematic of the pulse sequence is shown in Fig. 1a. After a slice-selective rf excitation, the moment of the slice selection gradient (G_{SS}) is refocused, and an FID signal is formed which is sampled during a short SG data acquisition. Next, the conventional phase encoding (G_{PE}) and readout gradients (G_{RO}) are applied, and the image data is recorded. Finally, the gradient moment in phase encoding direction is rewound, and a spoiler gradient is applied in slice selection direction.

Flow compensation

Two different flow compensation techniques were implemented to reduce flow artifacts in the images. A first order flow compensation was implemented, which nulls the first gradient moment

$$M_1(t) = \int_0^t G(t') \cdot t' \mathrm{d}t' \tag{1}$$

at the echo time. In a conventional, serial implementation (cFC) the flow compensation gradients are applied directly after the G_{SS} and prior to G_{RO}, respectively (Fig. 1b). Thus, both SG-signal and image data are flow-compensated. In the second, shorter implementation (sFC) symmetric bipolar flow compensation gradients are inserted in slice selection and readout direction, so that the first gradient moment is nulled only during the imaging part (Fig. 1c). The amplitude G of these compensating gradients is calculated according to

$$G = \sqrt[3]{\frac{1}{2}(-M_1) \cdot s_{\max}^2} \tag{2}$$

where $s_{\max}$ is the minimum rise time given by the hardware, and M_1 is the first moment of the other imaging gradients along the respective gradient axis. Equation 2 was derived assuming that the bipolar gradients have a vanishing plateau time t_p (i.e., triangular gradient shape). In the case that G exceeds the maximum gradient amplitude $G_{\max}$ of the MR system, the amplitude of the bipolar gradient was set to $G_{\max}$, and a non-vanishing plateau time t_p was calculated to be

$$t_p = -\frac{3}{2}\frac{G_{\max}}{s_{\max}} + \sqrt{\left(\frac{G_{\max}}{2 \cdot s_{\max}}\right)^2 - \frac{M_1}{G_{\max}}} \tag{3}$$

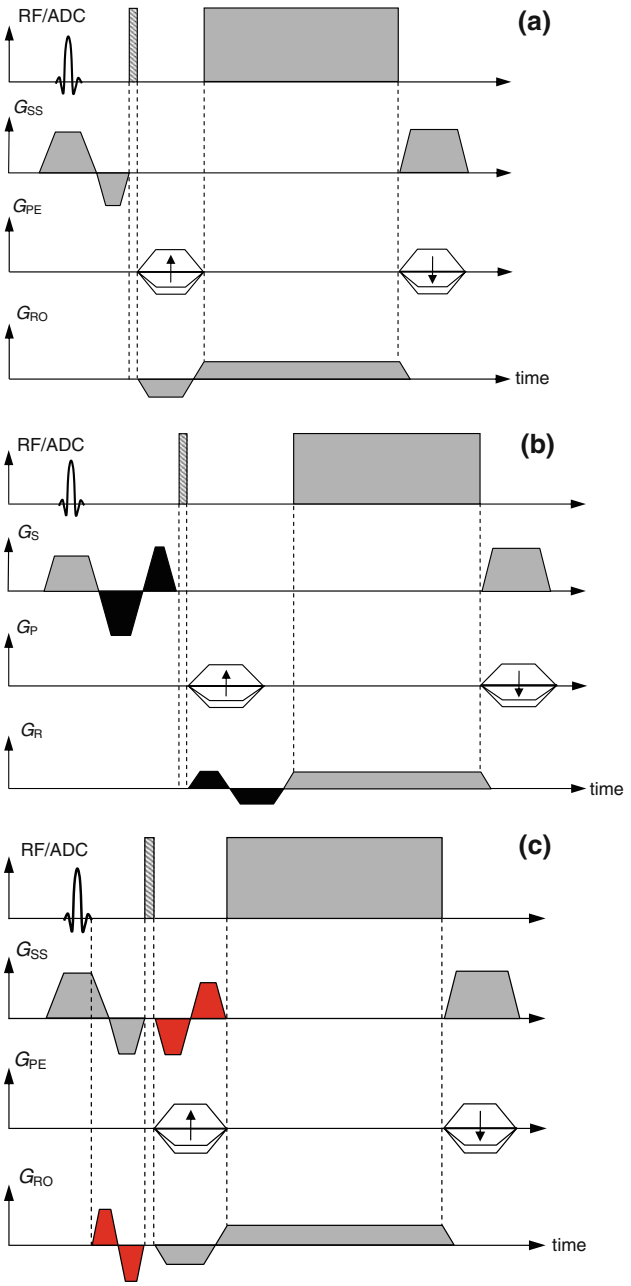

Fig. 1 Three variants of the SG implementation in a Cartesian 2D FLASH sequence. **a** In the noFC implementation the readout (RO) prewinders and the phase encoding (PE) gradients do not overlap with the refocusing gradients in slice selection (SS) direction and the SG-ADC (*dashed*) is inserted in-between. **b** With cFC additional gradients to null the first order moments are inserted (*black*). **c** In sFC, first moment nulling is achieved with bipolar gradients before and after the SG-ADC (*red*), respectively. Note, that these gradients do not null M_1 during the acquisition of the SG-ADC

Since the first moments in both slice selection and readout direction are not yet compensated, a larger variation of the SG signal at different times during the cardiac cycle is expected which might simplify the generation of a trigger event from the SG data.

If the bipolar sFC gradients are not longer than the imaging gradients applied simultaneously on the other gradient axes, the sFC implementation has the same duration as the SG sequence without flow compensation.

SG image reconstruction

A program for retrospective processing of the SG and image data was implemented in the programming language IDL (Version 6.3, Research Systems Inc., Boulder, CO). The following steps were implemented to reconstruct images at different cardiac phases:

For technical reasons, each SG signal consisted of not only 1 but 8 data points. To increase the SG signal intensity the absolute values of these 8 data points were added. Absolute rather than complex data averaging was chosen to avoid cancellation effects due to eddy current-induced phase shifts.

Since cardiac information is only contained in the signal variation over time, next, the time-average of the SG signal was subtracted. The signal was then bandpass-filtered with the non-recursive, digital filter provided by IDL to remove high frequency components from noise and low-frequency variations due to respiratory motion. For mice, the lower and upper frequency limits of the filter were set to 3 and 25 Hz, whereas in humans a frequency range of 0.5–10 Hz was chosen.

In the volunteer experiments, SG and image data were acquired with several coil elements. In a next pre-processing step, for each coil element the standard deviation (SD) of the normalized and filtered SG data as a function of time was calculated. Data from the coil channel that showed the highest SD was used as the SG signal, since the remaining signal variations were assumed to be caused by cardiac motion. Data of the different coils were not averaged, because it turned out that the SG-signal from other coil elements shows different variation properties and averaging leads to a reduction in signal variations. Exemplary normalized SG signals as a function of time are plotted in Fig. 2 for a volunteer and a mouse.

Next, cardiac trigger events were detected in the filtered SG data. As a start the maximum of the magnitude of the SG signal intensity during one expected heart cycle was defined as a trigger. Subsequent trigger events were generated using an auto-correlation algorithm. Therefore, a window of the length of one expected heart cycle was shifted over the SG signal, and the maximum of the cross correlation between this windowed SG data and an averaged SG signal of the first ten heart cycles was used to calculate the time point of the next trigger event. The acquired image data were then binned into different heart phases using the time information of the trigger events. If the same k-space line occurred various times in the same bin, the data was added and normalized.

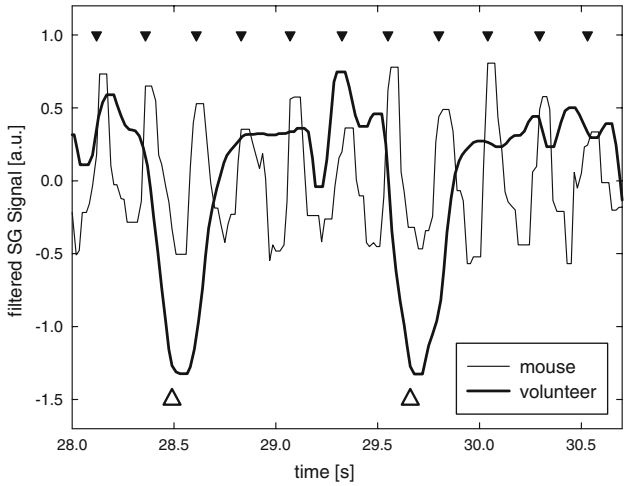

Fig. 2 Typical detail of the normalized and filtered noFC SG signals from a volunteer (*thick line*) and a mouse (*fine line*). The cardiac cycle of the mouse is about five times faster than that of the volunteer. Times of detected trigger events are marked with *triangles*

The images were reconstructed with the conventional sum-of-squares image reconstruction for multiple coil elements.

Volunteer experiments

In ten healthy volunteers (six males, four females, mean age 26 years, range 22–29 years) 4-chamber-views of the heart were recorded with each of the three pulse sequence variants. The 4-chamber-view promises a higher flow-sensitivity due to its more complex flow patterns compared to other orientations (both through and in-plane). MR data was received with a six channel body anterior and a six channel body posterior coil array. Eight SG data points were acquired with a bandwidth of 80 Hz/pixel (SG-ADC). For the imaging part, the following parameters were used: FOV $= 340 \times 276\,\mathrm{mm}^2$, matrix $= 256 \times 256$, slice thickness $= 8.0$ mm, $\alpha = 15°$, bandwidth $= 130\,\mathrm{Hz/pixel}$, symmetric echo. The minimal possible TR and TE values of 18 and 12.6 ms of the longest cFC sequence were chosen for all three pulse sequence variants to assure direct comparability between the signal intensities. To be able to reconstruct images at all times in the cardiac cycle, each k-space line was acquired 80 times so that even at very long RR-intervals of $80 \times 18\,\mathrm{ms} = 1.44\,\mathrm{s}$ sufficient image data were available. To demonstrate the effect of the flow compensation the protocol parameters were selected such that the resulting images were highly sensitive to flow artifacts. Therefore, high first moments of the imaging gradients were generated which resulted in a flow sensitivity of VENC $= 45$ and 55 cm/s in slice selection and readout direction, respectively, where

$$\text{VENC (velocity encoding)} = \frac{\pi}{\gamma\,|\Delta M_1|} \tag{4}$$

with γ being the gyromagnetic ratio. By definition, when the velocity component along the gradient direction is equal to $\pm$VENC, the resulting phase difference is $\pm\pi$. At optimal imaging parameters (i.e., shorter gradient timing) a higher VENC would be present which leads to a more homogeneous signal in the ventricle. For comparison, additionally the ECG signal was recorded with an MR-compatible ECG triggering unit.

The data was analyzed for differences in the SG signal of the three implementations, for differences of the triggers derived using SG or ECG, respectively, and for the effects of FC. The SD of the SG signals was calculated. It was assumed that a higher SD corresponds to a higher sensitivity of the signal to the physiological motion. To determine the reliability of the SG trigger, the SD of the time difference between SG trigger event and corresponding ECG trigger event was calculated.

To assess the effect of the FC, image data were reconstructed with a temporal resolution of 25 ms using the ECG signal for triggering. A circular region of interest (ROI) with a diameter of 40 pixels was placed in the left heart chamber and the mean signal intensity S_{mean} within this ROI was calculated for each heart phase. For comparison, an average over 30 heart phases was calculated. For one volunteer with an extremely short heart cycle of down to 600 ms only 24 heart phases could be reconstructed and the average was calculated from these. To allow for an easier comparison, S_{mean} is given in percent of the noFC result.

Animal experiments

Experiments were also carried out on four mice (two CD1 nude mice, two C57BL/6 mice, body weight 30 g) on the same clinical 1.5 T MR system using a home-built small animal Tx/Rx solenoid coil (inner diameter 26 mm, length 100 mm). Animals were anesthetized with 1.5% isoflurane since Kober et al. [20] showed that, compared to ketamine/xylazine, isoflurane is advantageous for small-animal MR studies of the heart because it better maintains cardiac function.

The following protocol parameters were used: FOV $= 50 \times 50\,\mathrm{mm}^2$, matrix $= 256 \times 256$, slice thickness $= 1.5$ mm, $\alpha = 25°$, BW $= 130\,\mathrm{Hz/pixel}$, echo asymmetry $= 12.5\%$. Due to the significantly shorter RR-interval of the animals, only 30 repetitions were acquired for each k-space data set. The TR/TE for the three pulse sequences were 17/7.6 ms (noFC), 21/11.2 ms (cFC), and 18/8.64 ms (sFC), which resulted in a total scan time of 130 s (noFC), 162 s (cFC), and 139 s (sFC). In the animal experiments the minimal TR/TE times for each sequence variant were chosen. To make use of the maximum gradient amplitudes of 30 mT/m, slices were not angulated and a transverse slice position through the heart was chosen.

Table 1 Mean SD of the filtered and normalised SG signals of volunteers and mice as a function of the sequence variant

	SD of the SG signal		
	noFC	cFC	sFC
Volunteers	0.46 ± 0.07	0.33 ± 0.07	0.46 ± 0.08
Animals	0.24 ± 0.11	0.28 ± 0.14	0.25 ± 0.12

Table 2 Mean SD of the time difference between trigger events derived from the ECG-signal and from the SG signal for all three sequence variants

SD of mean time difference (s)		
noFC	cFC	sFC
0.02 ± 0.02	0.11 ± 0.15	0.013 ± 0.005

The SD of the SG signals from the three implementations was calculated to compare the sensitivities of the signals to motion. To investigate the effect of flow compensation, six heart phases were reconstructed using a trigger derived from the SG signal, and S_{mean} of a ROI covering the entire heart of the animal was calculated for each heart phase.

Results

Volunteer experiments

The mean heart cycle of the volunteers was in the range of 600–1400 ms. In Table 1, the average SD of the SG signals of all sequence variants are listed. Compared to the SD of the noFC implementation, the SD of the cFC implementation is significantly lower (paired t test: $P = 0.002$) whereas the SD of the noFC and the sFC implementation are equivalent ($P = 1.0$).

The mean time difference between ECG and SG trigger events varies individually and between sequence variants. Table 2 lists the average SD of this time shift for each sequence variant. The highest SD is observed in the cFC variant. In two volunteers, in 49 and 59 ECG events no corresponding SG events could be detected, and for the remaining data a SD of 0.39 s was found. In all other volunteers, only up to three SG events were not detectable. In contrast, the SG data from both noFC and sFC variant provided reliable triggers in all volunteers with average SD of 0.02 and 0.005 s, respectively.

In Fig. 3 mean signal intensity S_{mean} in a ROI is plotted for one volunteer as a function of the heart phase as an example. Both flow-compensated techniques cFC and sFC yield comparable results. The noFC data show a strong reduction

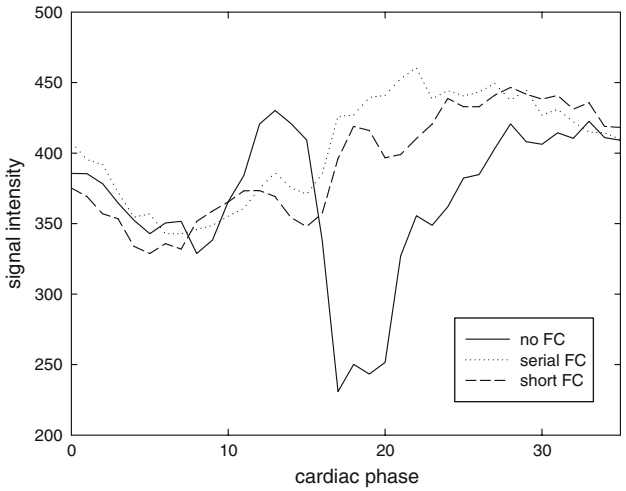

Fig. 3 Signal intensity S in the ROI in the left heart chamber of a volunteer over the heart phase for all three sequence variants—one cardiac phase lasts 25 ms

between the 15th and 25th heart phase which is not present in the flow-compensated SG data.

The average S_{mean} in the ROI in the left heart chamber are given in Table 3. All values are normalized to the value of the noFC implementation. The results show that S_{mean} significantly increases in the flow compensated sequence variants (a paired t test between the noFC and the cFC/sFC values results in $P = 0.0038/0.0001$).

MR images of the heart phase from 500 to 525 ms after the ECG trigger are shown for one volunteer for all three sequence variants in Fig. 4. All images were acquired under free breathing which explains the ghosting artifacts of the chest wall. The flow artifacts are strongly pronounced in the noFC sequence, and structures in the heart are hardly distinguishable. In contrast, in both flow compensation sequences the two heart chambers and atria can clearly be identified, the septum can be distinguished and ghosting in phase encoding direction is reduced.

In the volunteer experiments the resulting SG sequence timing was suboptimal for clinical cardiac imaging as very long TE times were used. Using an echo asymmetry of 12.5%, maximum gradient amplitudes and slew rates as well as optimized RF-pulses, TE could be reduced to 3.0/4.2/3.6 ms for the noFC/cFC/sFC volunteer protocols, respectively, which would be acceptable for clinical use. However, in this study sequence parameters were intentionally chosen to demonstrate the effect of flow compensation, and therefore the images were highly flow sensitive.

Animal experiments

The mean heart cycle of the animals was found to be 130–230 ms. As the bipolar compensating gradients are about

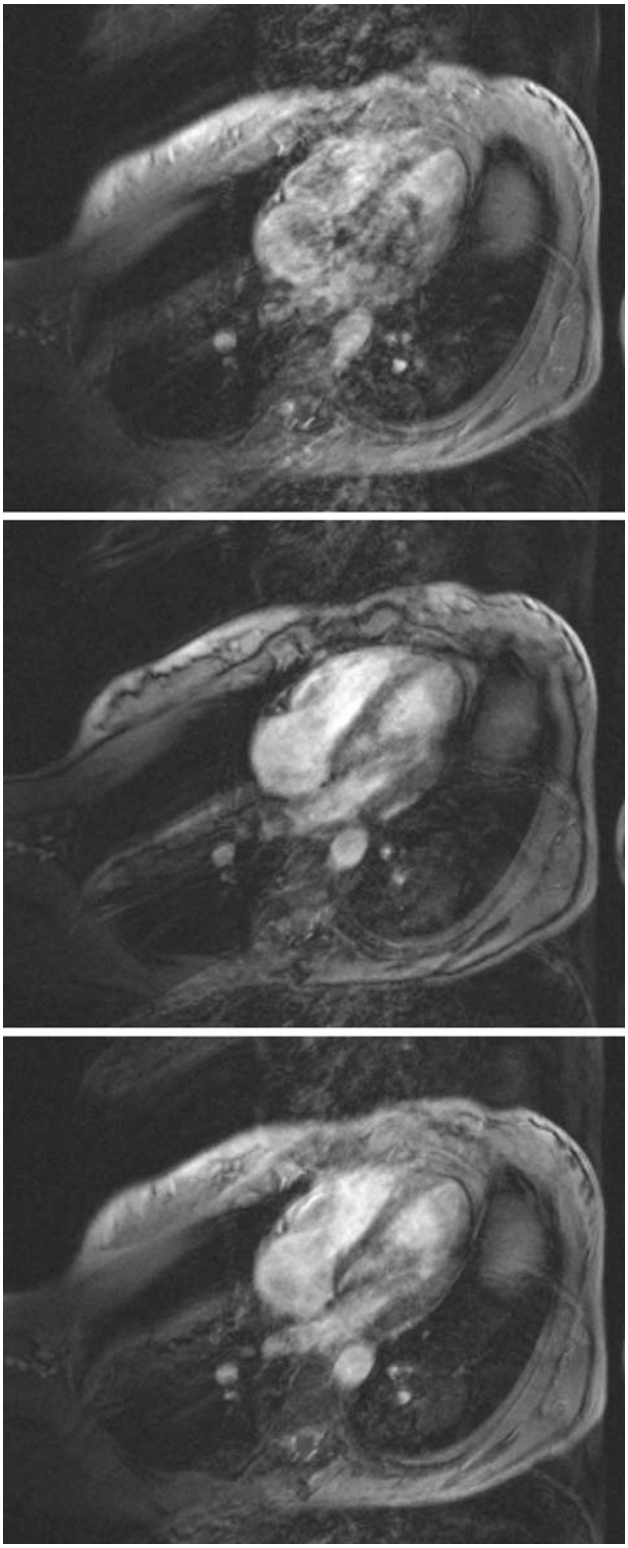

Fig. 4 ECG-gated MR images from all three sequence variants of the heart phase 500–525 ms after the ECG trigger event in one volunteer. The noFC variant (*top*) shows strong flow artifacts, and structures in the heart are hardly distinguishable. In contrast, in the cFC (*middle*) and the sFC (*bottom*) sequence variant structures as the heart chambers and the septum are clearly visible. The images still contain ghosting artifacts from breathing motion

Table 3 Mean value of S_{mean} of a ROI in the heart for volunteers and animals for all three sequence variants

	S_{mean} (%)		
	noFC	cFC	sFC
Volunteers	100	119 ± 16	115 ± 8
Animals	100	111 ± 11	110 ± 13

The signal intensities are given in percent of the intensity in the respective noFC experiment

1 ms longer than the gradients in the other directions, TR and TE of sFC is prolonged accordingly over the noFC variant; however, cFC is an additional 30%/17% longer than sFC in TE/TR.

The SD of the SG signals of all sequence variants are listed in Table 1. No difference in the SD of the sequence variants could be observed in the animals. Table 3 gives the results for the average S_{mean} in the animals, which is found to be higher in the flow compensated sequence variants, however, due to the low number of measurements no statistical analysis was performed.

In Fig. 5, MR images of one heart phase in a mouse are shown for each sequence variant. As the SG-ADC data was used for triggering, heart phases had to be chosen manually. Increased signal intensity is observed in the flow-compensated variants; however, regions with low signal intensities are still visible, which are reduced in size over the noFC variant.

The results of the animal experiments show that the sFC variant is faster by 23% than the cFC in TE. Compared to the variant without flow compensation, a prolonged sequence timing was observed as the bipolar flow compensation gradients exceeded the imaging gradients by about 1 ms. In general, the duration and amplitudes of the bipolar gradients are a complicated function of the hardware parameters G_{max} and s_{max} and the measurement parameters such as FOV, matrix size, and slice thickness which influence the first moment to be compensated. Nevertheless, with the presented sFC technique always a shorter gradient timing could be achieved compared to the serial cFC.

Discussion

In this work, a time-efficient flow-compensation technique sFC for a 2D FLASH SG sequence was presented. The sFC method was compared to sequence variants without flow-compensation and a conventional, serial flow-compensation implementation.

In the volunteer images strong ghosting artifacts were present which partially obscured important anatomical structures. In principle, the SG data could also be used to reduce

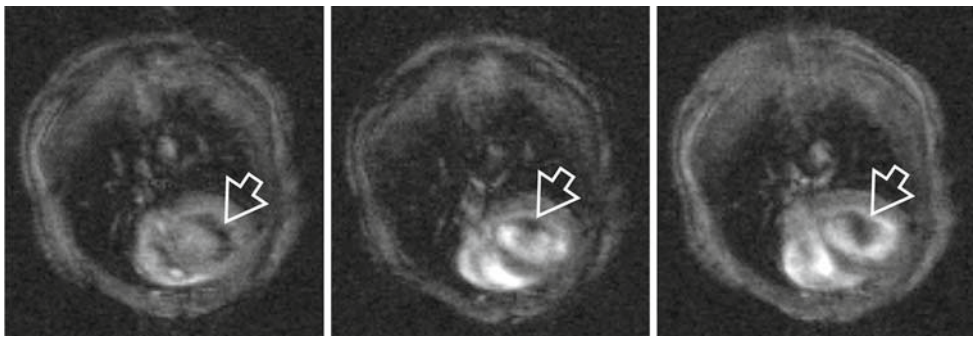

Fig. 5 SG-gated MR images of corresponding heart phases of a mouse recorded with the noFC (*left*), the cFC (*centre*) and the sFC (*right*) sequence variant. Both flow compensation variants improve image quality, but signal dephasing (*arrow*) is still visible in the heart chamber

these respiratory artifacts [11]. To perform retrospective respiratory gating imaging information for all phases of the respiratory cycle are needed, which requires significantly longer total acquisition times [21] as were used in these experiments. However, the analysis of the effect of the flow compensation was not affected by the ghosting artifacts, and the improved image quality with flow compensation was clearly visible.

The filtered and normalized SG signal of the sFC variant showed a higher SD than the cFC variant in volunteers. The SD of the SG signal was taken as a measure for its sensitivity to motion, since SG data are a spatial average over the MR signal in the vicinity of the coil. Thus, in addition to its time-effectiveness, the sFC technique has the advantage over the conventional implementation that the sensitivity to physiological motion is increased. An increased motion sensitivity of sFC is expected, as the first gradient moment during SG data acquisition is not compensated. Therefore, the MR signal from moving spins in the heart can destructively interfere with the signal from static regions, and these effects are highly dependent on the different flow velocities present during systole and diastole.

When comparing the SG and the ECG trigger times from the measurements on volunteers, it is notable that the mean time difference between both triggers is not constant but depends on sequence variant as well as on the volunteer. This is a systematic disadvantage of the SG technique because the SG trigger cannot be assigned to a particular cardiac time frame such as systole or diastole. The intra-volunteer and intra-measurement time difference in noFC and sFC is very stable, i.e. shows a small SD, whereas in some measurements the SD of the mean time difference of the cFC sequence variant is very high. This again illustrates that a more reliable trigger can be derived from SG data that are not flow-compensated.

In this analysis the ECG signal was taken as the gold standard. As discussed in the introduction trigger errors commonly occur when ECG triggering is used during MR imaging. However, if combined with appropriate imaging sequences, ECG triggering works accurately in most cases. Furthermore, in this study only healthy volunteers were examined, so that the ECG trigger can be considered to be a precise reference.

In this study, the image quality of the three sequence variants was not compared to a clinical standard pulse sequence for cardiac imaging such as breath-held ECG-gated CINE trueFISP, because the image contrasts of trueFISP and FLASH acquisitions are very different. Similarly, a comparison between the standard breath-held technique and the free-breathing acquisition was not performed, because this would predominantly provide information about the breathing artifacts, whereas this study intended to investigate the flow-related signal variations. Finally, the long acquisition times of several minutes made our image acquisitions prone to gross volunteer motion, whereas the short breath-held standard acquisitions are not affected by motion. Thus, a voxel-to-voxel comparison of the images would be difficult to perform. Instead, S_{mean} in a region of high flow was found to be a good indicator for the effectiveness of the flow compensation.

Without flow compensation, a reduction of S_{mean} is observed during phases with significant amount of motion in the volunteers. With first order flow compensation, the mean signal intensity S_{mean} during the whole heart cycle is higher. As shown in Table 3, the averaged values over the cardiac cycle in the volunteers are significantly higher with flow compensation. In the animal experiments, an increase of the average S_{mean} is also observed, but due to the low sample size no statistical significance can be deducted from the data. The MR images show that the regions of signal loss due to flow do not vanish completely in the cFC and sFC variants but are reduced in size. The implemented flow compensation only corrects for the velocity-dependent phase effects, and higher order terms associated with acceleration still create phase differences. This higher order intravoxel dephasing is more pronounced in small animals due to the limited gradient strength available on the whole-body MR system which leads to longer echo times. Therefore, in the animals the regions with signal loss due to flow still persist but are reduced in size with flow compensation. To overcome this limitation dedicated gradient inserts should be used [22].

In this study a clinical 1.5 T MR system with a dedicated small animal coil was used to image mice. Though challenging, the feasibility of small animal imaging was already demonstrated in various studies with similar experimental set ups, and spatial resolutions down to 100 μm or less were achieved [23–26]. Clinical MR systems are typically operating at lower field strength of 1.5–3 T as compared to dedicated small animal systems which reduces susceptibility artifacts. In addition, the translation of the results to human imaging is facilitated, since comparable imaging contrasts are observed and the same imaging protocols and post-processing software can be used.

Conventional flow compensation in slice selection/readout direction can be achieved with two additional gradients that balance both zeroth and first moment of the slice selection/readout gradients [27]. During these gradients an echo (i.e., a zero crossing of the zeroth moment) is formed, which could also be used to sample SG data. Such an implementation, though feasible, imposes restrictions upon the choice of SG receiver bandwidth, since SG data are acquired in the presence of a gradient. In our implementation, SG data are always acquired in the absence of gradient activity. Thus, SG data represent a true spatial average of the MR signal and the SG-SNR can be increased by averaging of multiple SG data points.

In our experiments, several advantages of the sFC technique were found: First, the SG signal of the sFC is more sensitive to physiological motion and thus more adequate to derive a trigger signal than the SG signal of the cFC implementation. Second, the sFC implementation results in a shorter overall sequence timing, which reduces the acquisition time and minimizes higher order motion artifacts. With this SG implementation it was possible to acquire time-resolved cardiac images on both volunteers and small animals on a clinical whole-body MR system.

Acknowledgments This work was supported by a grant from the German Federal Ministry of Education and Research (project EISENHERZ, 13N8895). We are also indebted to Manfred (Manni) Jugold, Sarah Floesser, and Monika Dadrich for their help with the animal experiments.

References

1. Togawa T, Okai O, Oshima M (1967) Observation of blood flow e.m.f. in externally applied strong magnetic field by surface electrodes. Med Biol Eng 5(2):169–70
2. Tenforde TS (2005) Magnetically induced electric fields and currents in the circulatory system. Prog Biophys Mol Biol 87(2–3): 279–288
3. Keltner JR, Roos MS, Brakeman PR, Budinger TF (1990) Magnetohydrodynamics of blood flow. Magn Reson Med 16:139–149
4. Rokey R, Wendt RE, Johnston DL (1988) Monitoring of acutely ill patients during nuclear magnetic-resonance imaging—use of a time-varying filter electrocardiographic gating device to reduce gradient artifacts. Magn Reson Med 6(2):240–245
5. Polson M, Barker A, Gardiner S (1982) The effect of rapid rise-time magnetic fields on the ECG of the rat. Clin Phys Physiol Meas 3:231–234
6. Shetty AN (1988) Suppression of radiofrequency interference in cardiac gated MRI—a simple design. Magn Reson Med 8(1):84–88
7. Damji A, Snyder R, Ellinger D, Witkowski F, Allen P (1988) RF interference suppression in a cardiac synchronization system operating in a high magnetic field NMR imaging system. Magn Reson Imaging 6:637–640
8. Wendt RE, Rokey R, Vick W, Johnston DL (1988) Electrocardiographic gating and monitoring in NMR imaging. Magn Reson Imaging 6:89–95
9. Fischer EF, Wickline SA, Lorenz CH (1999) Novel real-time R-wave detection algorithm based on the vectorcardiogram for accurate gated magnetic resonance acquisitions. Magn Reson Med 42:361–370
10. Kugel H, Bremer C, Puschel M, Fischbach R, Lenzen H, Tombach B, Van Aken H, Heindel W (2003) Hazardous situation in the MR bore: induction in ECG leads causes fire. Eur Radiol 13(4):690–694
11. Brau AC, Brittain JH (2006) Generalized self-navigated motion detection technique: preliminary investigation in abdominal imaging. Magn Reson Med 55:263–270
12. Crowe ME, Larson AC, Zhang Q, Carr J, White RD, Li D, Simonetti OP (2004) Automated rectilinear self-gated cardiac cine imaging. Magn Reson Med 52(4):782–788
13. Nijm GM, Sahakian AV, Swiryn S, Larson AC (2007) Comparison of signal peak algorithms for self-gated cardiac CINE MRI. Comput Cardiol 34:407–410
14. Larson AC, White RD, Laub G, McVeigh ER, Li D, Simonetti O (2004) Selfgated cardiac cine MRI. Magn Reson Med 51:93–102
15. Hiba B, Richard N, Janier M, Croisille P (2006) Cardiac and respiratory double self-gated cine MRI in the mouse at 7 T. Magn Reson Med 55:506–513
16. Pattany PM, Phillips JJ, Chiu LC, Lipcamon JD, Duerk JL, McNally JM, Mohapatra SN (1987) Motion artifact suppression technique (MAST). Comput Assist Tomogr 11(3):369
17. Haacke EM, Lenz GW (1987) Improving MR image quality in the presence of motion by using rephasing gradients. Am J Roentgenol 148:1251–1258
18. Wendt RE III (1991) Interactive design of motion-compensated gradient waveforms with a personal computer spreadsheet. J Magn Reson Imaging 1(1):87–92
19. Wood ML, Henkelman MR (1999) Artifacts: In: Stark DD, Bradley WG (ed) Magnetic resonance imaging(1). St. Louis, Mosby, Chap. 10
20. Kober F, Iltis I, Cozzone PJ, Bernard M (2004) Cine-MRI assessment of cardiac function in mice anesthetized with ketamine/xylazine and isoflurane. Magn Reson Mater Phy 17:157–161
21. Ehman RL, McNamara MT, Pallack M, Hricak H, Higgins CB (1984) Magnetic resonance imaging with respiratory gating: techniques and advantages. Am J Radiol 143:1175–1182
22. Mayer D, Zahr NM, Adalsteinsson E, Rutt B, Sullivan EV, Pfefferbaum A (2007) In vivo fiber tracking in the rat brain on a clinical 3T MRI system using a high strength insert gradient coil. Neuroimage 35(3):1077–1085
23. Fink C, Kiessling F, Bock M, Lichy MP, Misselwitz B, Peschke P, Fusenig NE, Grobholz R, Delorme S (2003) High-resolution 3D MR angiography of rodent tumors: morphologic characterization of intratumoural vasculature. J Magn Reson Imaging 18:59–65
24. Kobayashi H, Kawamoto S, Saga T, Sato N, Hiraga A, Konishi J, Togashi K, Brechbiel MW (2001) Micro-MR angiography of normal and intratumoral vessels in mice using dedicated

intravascular MR contrast agents with high generation of polyamidoamine dendrimer core: Reference to pharmacokinetic properties of dendrimer-based MR contrast agents. J Magn Reson Imaging 14:705–713

25. Kiessling F, Greschus S, Michy MP, Bock M, Fink C, Vosseler S, Moll J, Mueller MM, Fusenig NE, Traupe H, Semmler W (2004) Volumetric computed tomography (VCT): a new technology for noninvasive, high-resolution monitoring of tumor angiogenesis. Nat Med 10(10):1133–1138
26. Franco F, Thomas GD, Giroir B, Bryant D, Bullock MC, Chwialkowski MC, Victor RG, Peshock RM (1999) Magnetic resonance imaging and invasive evaluation of development of heart failure in transgenic mice with myocardial expression of tumor necrosis factor-alpha. Circulation 99:448–454
27. Bernstein MA, Shimakawa A, Pelc NJ (1992) Minimizing TE in moment-nulled or flow-encoded two- and three-dimensional gradient-echo imaging. J Magn Reson Imaging 2:583–588